Complex plume stoichiometry during pulsed laser deposition of $SrVO_3$ at low oxygen pressures

Jun Wang, Guus Rijnders, and Gertjan Koster

Citation: Appl. Phys. Lett. **113**, 223103 (2018); doi: 10.1063/1.5049792
View online: https://doi.org/10.1063/1.5049792
View Table of Contents: http://aip.scitation.org/toc/apl/113/22
Published by the American Institute of Physics

Articles you may be interested in

Nanoscale oxygen ion dynamics in $SrFeO_{2.5+\delta}$ epitaxial thin films
Applied Physics Letters **113**, 221904 (2018); 10.1063/1.5046749

Two distinct surface terminations of $SrVO_3$ (001) ultrathin films as an influential factor on metallicity
Applied Physics Letters **113**, 171601 (2018); 10.1063/1.5051434

Excellent structural, optical, and electrical properties of Nd-doped $BaSnO_3$ transparent thin films
Applied Physics Letters **113**, 202102 (2018); 10.1063/1.5063538

Characteristic investigation of a flexible resistive memory based on a tunneling junction of Pd/BTO/LSMO on mica substrate
Applied Physics Letters **113**, 223501 (2018); 10.1063/1.5054040

Inhomogeneous barrier heights at dipole-controlled $SrRuO_3$/Nb:$SrTiO_3$ Schottky junctions
Applied Physics Letters **113**, 221603 (2018); 10.1063/1.5052712

Thermal conductivity in self-assembled $CoFe_2O_4$/$BiFeO_3$ vertical nanocomposite films
Applied Physics Letters **113**, 223105 (2018); 10.1063/1.5049176

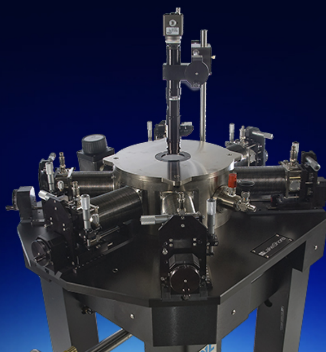
Cryogenic probe stations
for accurate, repeatable
material measurements

Complex plume stoichiometry during pulsed laser deposition of $SrVO_3$ at low oxygen pressures

Jun Wang, Guus Rijnders, and Gertjan Koster[a)]
Faculty of Science and Technology and MESA+ Institute for Nanotechnology, University of Twente, 7500 AE Enschede, The Netherlands

(Received 25 July 2018; accepted 6 November 2018; published online 27 November 2018)

To control the pulsed laser deposition synthesis, knowledge on the relationship between the plasma plume and the grown thin film is required. We show that the oxidation of species in the plasma plume still affects the $SrVO_3$ growth even at low oxygen partial pressures. Optical emission spectroscopy measurements for the plasma plume at different growth conditions were correlated with the film properties determined by Atomic force microscopy, X-ray diffraction, and transport. At reducing oxygen pressures, the background argon pressure can affect the oxidation in the plasma plume, which in turn controls the growth kinetics, stoichiometry, and electrical properties of the films. © *2018 Author(s). All article content, except where otherwise noted, is licensed under a Creative Commons Attribution (CC BY) license (http://creativecommons.org/licenses/by/4.0/).*
https://doi.org/10.1063/1.5049792

Transition metal oxides with the perovskite structure have received a lot of interest in recent years due to their broad range of properties, such as metal-to-insulator transitions, ferroelectricity, and superconductivity. These properties open the way for novel applications, for example, transistors, switches, and sensors.[1–3]

The material properties of thin films are related to surface morphology and crystal quality, which in turn are mostly determined by surface growth kinetics. Pulsed laser deposition (PLD) is a widely used thin film deposition technique. One of the most cited reasons for its popularity is that it enables the deposition of a broad range of materials that can be stoichiometrically transferred from targets to substrates. However, in reality, the exact distribution and nature of species that are being transferred, and their influence on the surface kinetics and growing films are still little known. The most generally adopted model is that the kinetic energy of the arriving species is the key parameter to determine the type of the growth mechanism.[4,5] The relationship between the ambient gas pressure and kinetic propagation characteristics of the expanding plasma plume is well-known: the plasma propagation behaviour evolves from thermalized to drag with the increasing background gas pressure.[6,7] The model suggests that the increased kinetic energy of the species at lower background gas pressures improves surface diffusion which is favourable to the crystallinity and the smoothness of the films.[8,9] More recent work has shown that oxidation of the arriving species also plays a role in controlling the smoothness and stoichiometry of the grown films.[10] In the pressure range where the kinetic transition occurs, the authors investigated the $SrTiO_3$ growth at varying oxygen pressures in the range from 0.01 mbar to 0.1 mbar. In contrast to the kinetic model, this work showed that stoichiometric and smooth films were obtained at higher oxygen pressures. The titanium atoms are oxidized to TiO_2 in the plasma plume at increased oxygen pressure, and Ti^{4+} is the most steady oxidation state for Titanium. Based on previous studies of plasma chemistry and thin film growth, which were conducted at relatively high absolute oxygen pressure, the question addressed in this study is whether oxidation of species plays any role at much lower oxygen pressure. $SrVO_3$ is a good material system to study the influence of the growth parameters on oxide thin film characteristics such as stoichiometry and surface morphology in a low oxygen pressure range. $SrVO_3$ can only be grown at very low oxygen (partial) pressure since over-oxidized V^{5+} hampers perovskite $SrVO_3$ to be formed. V^{4+} in $SrVO_3$ has tendency to dismutate: V^{4+} can be over-oxidized to V^{5+} at high oxygen pressure, and oxygen vacancies can also be formed under reducing conditions.[11,12] $SrVO_3$ recently gains a lot of attention due to its high electrical conductivity.[12,13] Although $SrRuO_3$ has been widely used as an electrode layer in the oxide thin film heterostructure and this material fulfils most requirements in many applications,[14–18] a much lower resistance is still desired for high frequency applications to reduce conduction losses. $SrVO_3$ has also been studied recently as a transparent conductor[19] and has been widely studied in theoretical modes as a correlated system.[20,21] To investigate whether the nature of species has an influence on the thin film growth at low oxygen pressure, we grew the $SrVO_3$ films at varying total pressures or varying oxygen partial pressures.

For a typical used target-to-substrate (T-S) distance of 50 mm, the change in kinetic propagation behaviour of the species occurs above 0.01 mbar.[7,10] At low oxygen pressure, an argon pressure was introduced to control the propagation of the expanding plasma plume. All of thin films were grown using a PLD system equipped with reflection high energy electron diffraction (RHEED). During growth, all films were monitored using RHEED to study the growth kinetics and the in-plane crystal structure. A thermal and chemical treatment was applied to achieve the single TiO_2 terminated $SrTiO_3$ (100) (STO) substrates.[22] A KrF excimer laser ($\lambda = 248$ nm) at a fluency of 2 J/cm^2 and a repetition rate of 1 *Hz* was used. Temperature was kept at 600 °C. Four

[a)]Electronic mail: g.koster@utwente.nl

 © Author(s) 2018.

samples in the first set were grown in the argon pressures of 0.01 mbar, 0.02 mbar, 0.025 mbar, and 0.04 mbar with the same oxygen partial pressure of 1×10^{-5} mbar. The second set of samples were deposited in the 0.025 mbar argon pressure with different oxygen partial pressures of 1×10^{-6} mbar, 5×10^{-6} mbar, and 1×10^{-5} mbar. With a constant background total pressure, and only varying the oxygen partial pressure, we should be able to separate the effects of oxidation and plasma species kinetics. The thickness of the films is kept at about 30 nm in this study.

Atomic force microscopy (AFM) (Bruker) in the tapping mode was used for characterizing the topography of the obtained films, which indicates the type of the growth mechanism. X-ray diffraction (XRD) (Xpert panalytical MRD) was used to characterize the crystal structure of the thin films. The out-of-plane lattice constant can be derived by performing $2\theta/\omega$ symmetrical scans around the (002) Bragg reflection of the $SrTiO_3$ substrate to indicate the stoichiometry of grown films. Transport properties were measured in the van der Pauw geometry using a Quantum Design Physical Properties Measurement System (QD PPMS) in the temperature range of 2 K–300 K.

To correlate the changes in nature of species being transferred with crystallinity and smoothness of the films, optical emission spectroscopy (OES) measurements for the $SrVO_3$ plume were performed at the thin film growth conditions. An intensified charge coupled device (ICCD) camera (Andor New iStar) connected with a spectrograph (Andor's Shamarock) was used to collect the data. The targets of SrO, V_2O_5, and V_2O_3 were also inspected to get information about the individual element in $SrVO_3$. The wavelength scale was calibrated using reference database.[23] We focus on the wavelength in the range from 470 nm to 530 nm for neutral Strontium and in the range from 600 nm to 640 nm for oxidized Vanadium. A bandpass of 257 nm and a spectral resolution of 1.5 nm can be obtained by using a 1024×1024 pixel array and a 300 lines/mm grating. Each spectrum was taken at different delay times τ after the target ablated.

Figure 1 shows AFM images and the corresponding cross-sectional profiles of the samples grown at argon pressures ranging from 0.01 mbar to 0.04 mbar with the oxygen partial pressure of 1×10^{-5} mbar. The insets correspond to the RHEED diffraction patterns in the [01] direction after growth. The films grown at pressures below 0.025 mbar have an island morphology, and the step-terrace structure of the substrate is barely visible [see Figs. 1(a) and 1(b)]. The corresponding RHEED patterns are so-called streaky patterns, which are indicative of a still relatively two dimensional flat and crystalline surface. The peak-to-peak height difference is about 0.5 nm for these films as seen in the cross-sectional profiles. On the other hand, the step-terrace structure is more clearly observed for the film grown at 0.025 mbar [shown in Fig. 1(c)]. Presumably, step-flow-like growth has occurred at the latter condition. The RHEED specular intensity versus time for this film is shown in Fig. S1, which additionally supports step-flow-like growth. The cross-sectional profile shows that the peak-to-peak height difference is about 1 nm. This value is higher than that in the previous two samples because in addition to the flat terraces, the image also reveals trenches at the edge of each terrace. Their origin is not fully understood; however, similar trenches have been seen in $SrRuO_3$ thin films, which are related to the surface termination.[14] Finally, Fig. 1(d) shows that 3D islands are formed for the film deposited at 0.04 mbar, with heights of more than 4 nm. It is also confirmed by RHEED showing a 3D transmission pattern.

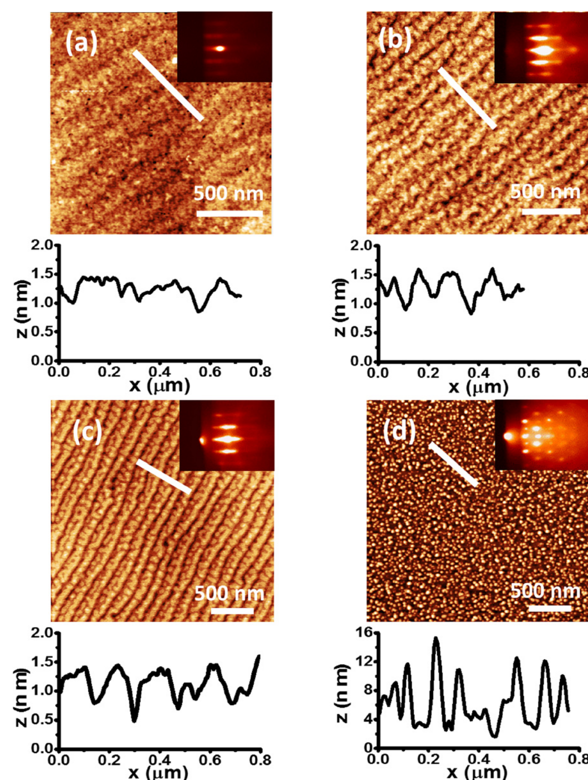

FIG. 1. AFM images of the $SrVO_3$ thin film grown at the same oxygen partial pressure of 1×10^{-5} mbar and varying argon background pressures of (a) 0.01 mbar, (b) 0.02 mbar, (c) 0.025 mbar, and (d) 0.04 mbar. Each inset shows the RHEED pattern, and a cross-section at each white line is shown below the AFM image.

Figure 2 shows AFM images of the films grown at varying oxygen partial pressures of 1×10^{-6} mbar, 5×10^{-6} mbar, and 1×10^{-5} mbar with the constant argon pressure of 0.025 mbar. AFM images show a layer-by-layer growth mode for the film grown at the 1×10^{-6} mbar and 5×10^{-6} mbar. At 1×10^{-6} mbar, Fig. 2(a) shows that the initial terrace morphology of the substrate surface is still visible. However, the morphology consists of very small islands on the terraces. The islands are too small to cover the terrace

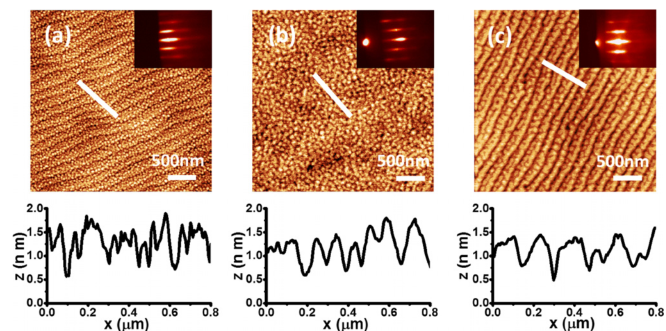

FIG. 2. AFM images of the $SrVO_3$ thin film grown at oxygen partial pressures of (a) 1×10^{-6} mbar, (b) 5×10^{-6} mbar, and (c) 1×10^{-5} mbar with the same argon pressure of 0.025 mbar. Each inset shows the RHEED pattern, and a cross-section at each white line is shown below the AFM image.

edge in the substrate. The cross-sectional profile shows that the peak-to-peak difference is about 1 nm. The inset RHEED pattern shows a streaky pattern. The arriving species are more likely to be nucleated in Fig. 2(b). The size of islands in Fig. 2(b) is larger than that of islands in Fig. 2(a). The large islands appear to cover the terrace edges explaining the absence of surface imprint of the substrate vicinal steps. The peak-to-peak difference is 1 nm as shown in the cross-sectional profile. The inset RHEED pattern also shows a so-called streaky pattern. Figure 2(c), the same image as shown in Fig. 1(c), shows a clear step-terrace structure for the film grown at 1×10^{-5} mbar. This is an evidence for a step-flow-like growth mode. The Kikuchi lines are visible in the corresponding RHEED pattern, which indicates a highly ordered surface.

Figure 3(a) shows XRD 00l scans around the (002) Bragg reflection of $SrTiO_3$ for the films grown at varying argon pressures. AFM images of these samples are shown in Fig. 1. The (002) film peaks of $SrVO_3$ are indicated by black arrows. The measurements are fitted using the Stepanov model for quantitative analysis,[24] and the corresponding out-of-plane lattice parameters are shown in Table I. The reciprocal mapping around $SrTiO_3$ (103) (see Fig. S2) showed that the $SrVO_3$ film is fully in-plane strained by the $SrTiO_3$ substrate. The equi-biaxial strain in the film plane due to the lattice mismatch between STO (3.905 Å) and SVO (3.842 Å) is 1.64%. Assuming that Poisson's ratio for SVO is 0.28 (Ref. 12), the expected out-of-plane lattice parameter for the stoichiometric SVO film is 3.793 Å. An increase in the film c-axis length corresponds to an increase in the unit cell volume which is caused by cation nonstoichiometry or point defects in the lattice.[10,12] As the out-of-plane lattice parameter decreases with the increasing argon pressure, the film grown at higher pressure is closer to stoichiometry. The Laue fringes around the film peaks originating from the coherence between individual layers in the film are observed for the film grown at 0.01 mbar, 0.02 mbar, and 0.025 mbar, which also indicate a high degree of crystallinity. The thickness d of the grown film, listed in Table I, can also be derived from the spacing of the Laue fringes.

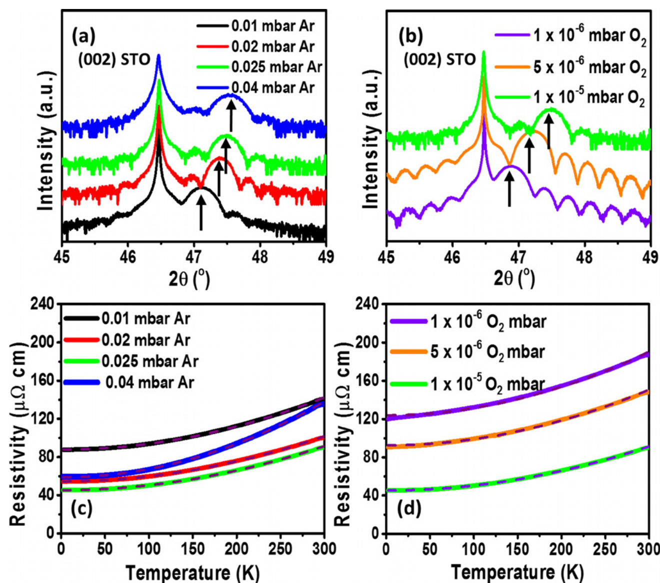

FIG. 3. XRD 00l scans around the (002) Bragg reflection of $SrTiO_3$ for the $SrVO_3$ thin film grown at (a) an oxygen partial pressure of 1×10^{-5} mbar with the varying argon pressures and (b) at an argon pressure of 0.025 mbar with the varying oxygen partial pressures. $SrVO_3$ film peaks are indicated by black arrows. Temperature-dependent resistivity ρ for deposited $SrVO_3$ films grown at (c) varying argon pressures and (d) varying oxygen partial pressures. The purple dashed line shows the fitting of $\rho = \rho_0 + AT^2$ for each film.

TABLE I. Overview of lattice parameters and thickness derived from the XRD scans for all samples.

P_{Ar}/P_{O_2} (mbar)	C_{axis} (Å)	d (nm)	No. of pulses
$0.01/1 \times 10^{-5}$	3.853 ± 0.001	31.0 ± 0.5	900
$0.02/1 \times 10^{-5}$	3.833 ± 0.001	34.0 ± 0.2	950
$0.025/1 \times 10^{-5}$	**3.826 ± 0.001**	**31.0 ± 0.2**	**900**
$0.04/1 \times 10^{-5}$	3.819 ± 0.001	30.0 ± 0.5	900
$0.025/1 \times 10^{-6}$	3.870 ± 0.001	30.0 ± 0.2	900
$0.025/5 \times 10^{-6}$	3.846 ± 0.001	30.0 ± 0.2	900

Figure 3(b) shows the XRD 00l measurement of films grown at varying oxygen partial pressures. AFM images of these samples are shown in Fig. 2. The out-of-plane lattice parameter and the thickness for the obtained films are shown in Table I using the same fitting algorithm. Again, an increased thin film c-axis length corresponds to an increase in the unit cell volume which results from point defects in the lattice. The XRD results suggest that the films grown at increasing oxygen partial pressure get closer to the stoichiometric composition.

The temperature dependence of electrical resistivity was measured in the temperature range of 2 K–300 K, as shown in Figs. 3(c) and 3(d). All the samples show metallic behaviour: the resistivity decreases with the decreasing temperature. Furthermore, the electrical resistivity as a function of temperature can be fitted by a $\rho = \rho_0 + AT^2$ relation (see purple dashed line), which is characteristic of a Fermi liquid behaviour. The fitting parameters are reported in Table S1. The lowest resistivity of 90 $\mu\Omega$ cm at room temperature is obtained for the film with the smoothest surface and the best stoichiometry, which is grown at a 0.025 mbar argon pressure with the oxygen partial pressure of 1×10^{-5} mbar. In order to be able to convincingly exclude a contribution from the substrate, a bare STO substrate, which has been subjected to growth conditions of SVO, but without the actual deposition taking place, was measured by an insulation tester (Fluke 1507). The sample remained highly insulating with a resistivity of 146 MΩ cm. In addition, the same SVO thin film has been grown on the $(LaAlO_3)_{0.3}(Sr_2AlTa_6)_{0.7}$ (LSAT) substrate, a material that should not be reducible under any condition, at the optimal growth conditions. The resistivity of the film at room temperature is about 70 $\mu\Omega$ cm (see Fig. S3), which is even lower than the resistivity of the film grown on the STO substrate (90 $\mu\Omega$ cm). We think that these data can also be a strong evidence to rule out the contribution from the STO substrate.

To investigate the composition of the plasma plume at varying growth conditions, the optical emission spectroscopy (OES) measurement was performed on the expanding plume. Although these measurements only interpret the results qualitatively, they can still indicate the relative abundance of species in different growth conditions. To help identifying the spectrum for individual elements (Sr and V) in $SrVO_3$,

plasma using different targets of V_2O_3, V_2O_5, and SrO was imaged (shown in Fig. S4). Their images indicate that the spectra at the wavelength between 470 nm and 530 nm corresponds to neutral Strontium, and the spectra at the wavelength between 600 nm and 640 nm corresponds to oxidized Vanadium. The spectra of the oxidized Vanadium in the plasma plume of the $SrVO_3$ target are normalized by the maximum intensity of the plume expanding at 0.04 mbar, as shown in Fig. 4. $SrVO_3$ was ablated at varying total argon pressures of 0.01 mbar, 0.025 mbar, and 0.04 mbar with the same oxygen partial pressure of 1×10^{-5} mbar. At $\tau = 1.5$ μs, the intensity of all peaks corresponding to oxidized Vanadium is very low, since the species in plume mostly are neutral just after the target to be ablated. For the measurement at 0.01 mbar, the intensity of the peak at a wavelength of 620 nm does not change over time (see the black line). At 0.025 mbar and 0.04 mbar, presented in red and blue lines, the intensity of the peak at 620 nm rapidly increases after 4.5 μs. At $\tau = 5.5$ μs, the intensity of this peak for 0.04 mbar is higher than that of the peak for 0.025 mbar (see blue and red lines). The amount of the oxidized Vanadium in the plume increases with the increasing total argon pressure. This phenomenon is likely to be caused by the plume confinement due to scattering resulting from the increasing argon pressure. In addition, the plume expands more slowly at higher pressure, causing more species to be oxidized in the plasma plume.

The results from the structural investigation and the plasma plume analysis show the relationship between the thin film characteristics and the species in the plume. The XRD characterization shows that the c-axis of the grown films was dependent on the total argon pressure. It indicates that the stoichiometry of the thin films is the function of the increasing total pressure. The growth kinetics was indicated by the surface morphology study using AFM. At a 0.025 mbar argon pressure, presumably, step-flow-like growth mode has occurred, implying the improved surface diffusivity at this condition. However, the 3D growth mode occurred for the film grown at 0.04 mbar, indicating the limited mobility of particles at the substrate. The optimal room temperature resistivity of 90 $\mu\Omega\ cm$ was obtained for the film with the optimal crystalline structure and smooth surface morphology. The spectrum analysis indicates that the oxidized Vanadium in the plume was formed when the pressure increased to 0.025 mbar. An increased amount of oxidized species was observed at the pressure of 0.04 mbar. These

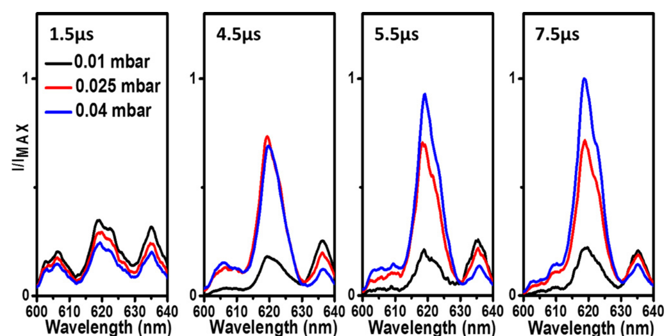

FIG. 4. The normalized spectra of the oxidized Vanadium in the plasma plume expanding of the $SrVO_3$ target.

correlations strongly suggest that the oxidized species in plasma plume are a necessary requirement for the stoichiometric growth of thin film of $SrVO_3$. The amount of oxidized species determines the surface diffusivity at the substrate for the films grown with the optimal at an argon pressure of 0.025 mbar. Apparently, an excess of oxidized species at an argon pressure of 0.04 mbar can cause the over-oxidation. We speculate that mostly 4+ Vanadium is necessary to obtain the perovskite phase of $SrVO_3$. The kinetic model proposed in previous works assumes that the diffusion activation energy increases with the increasing pressure.[8,9] The model assumes that changing kinetics of arriving species affects the surface diffusivity. However, in this work surface, smoothening and stoichiometric improvement are observed with the increasing background pressure up to 0.025 mbar. Therefore, we suggest that the enhanced surface diffusivity and improved stoichiometry are also dependent on oxidation of arriving species. A similar transition in the thin film stoichiometry and the surface morphology is observed for the films grown at varying oxygen partial pressures with the total pressure of 0.025 mbar. Since the kinetic energy does not change, this supports the model of having the oxidation of arriving species to be an important parameter to affect the thin film growth. This suggests that oxidation of arriving species not only could determine the surface diffusion energies but also could play a role in the competition between the formation of different phases, either through preferred nucleation or kinetically enhanced growth of island. These are topics for future investigations.

To further substantiate this model, in the supplementary material (see Figs. S6 and S7), the structural property and surface morphology of the film grown at varying target-to-substrate (T-S) distances are investigated. The total argon pressure and the oxygen partial pressure were kept at 0.035 mbar (higher than the optimal pressure observed in previous experiments) and 1×10^{-5} mbar, respectively. We observed the similar transition in the thin film stoichiometry and the surface morphology with the increasing T-S distance. A non-stoichiometry film was obtained at 28 mm. The step-flow-like growth occurred at the film grown at 42 mm, indicating the improved surface diffusivity by oxidized species. The 3D islands are observed for the film grown at 50 mm, implying an excess of the oxidized species. The plasma plume study suggests that the amount of oxidized species in the plume increases with the plume propagation from the target to the substrate at this pressure. This result also supports that surface diffusivity and film stoichiometry are dependent on oxidation of the arriving species at the substrate.

From the correlation between the thin film properties determined by AFM and XRD and the plasma plume composition analysed by OES measurements, we conclude that the surface diffusivity, growth kinetic, and the films stoichiometry are controlled by oxidation of arriving species. At reducing oxygen pressures, the spectrum of expanding plume indicates that the oxidation species in the plasma plume can be controlled by the total argon pressure, which in turn controls the quality of the thin films, including the electrical properties of $SrVO_3$.

See supplementary material for the reciprocal mapping of the $SrVO_3$ thin film, RHEED intensity of the thin grown in the optimal conditions, fitting parameters of resistivity as a function of temperature, optical emission spectroscopy spectra of plume of V_2O_3, V_2O_5, and SrO, and AFM and XRD studies of the films grown at varying T-S distances.

This work was supported by Nederlandse Organisatie voor Wetenschappelijk Onderzoek through Grant No. 13HTSM01.

[1]M. Imada, A. Fujimori, and Y. Tokura, Rev. Mod. Phys. **70**, 1039 (1998).
[2]I. H. Inoue and M. J. Rozenberg, Adv. Funct. Mater. **18**, 2289 (2008).
[3]H. W. Jang, A. Kumar, S. Denev, M. D. Biegalski, P. Maksymovych, C. W. Bark, C. T. Nelson, C. M. Folkman, S. H. Baek, N. Balke, C. M. Brooks, D. A. Tenne, D. G. Schlom, L. Q. Chen, X. Q. Pan, S. V. Kalinin, V. Gopalan, and C. B. Eom, Phys. Rev. Lett. **104**, 197601 (2010).
[4]G. Koster, G. J. H. M. Rijnders, D. H. A. Blank, and H. Rogalla, Appl. Phys. Lett. **74**, 3729 (1999).
[5]D. H. Blank, G. Koster, G. A. Rijnders, E. van Setten, P. Slycke, and H. Rogalla, J. Cryst. Growth **211**, 98 (2000).
[6]S. Amoruso, A. Sambri, and X. Wang, J. Appl. Phys. **100**, 013302 (2006).
[7]D. B. Geohegan, Thin Solid Films **220**, 138 (1992).
[8]P. R. Willmott, R. Herger, C. M. Schlepütz, D. Martoccia, and B. D. Patterson, Phys. Rev. Lett. **96**, 176102 (2006).
[9]J. E. Boschker, E. Folven, s. F. Monsen, E. Wahlström, J. K. Grepstad, and T. Tybell, Cryst. Growth Des. **12**, 562 (2012).
[10]R. Groenen, J. Smit, K. Orsel, A. Vailionis, B. Bastiaens, M. Huijben, K. Boller, G. Rijnders, and G. Koster, APL Mater. **3**, 070701 (2015).
[11]S. Hui and A. Petric, Solid State Ionics **143**, 275 (2001).
[12]J. A. Moyer, C. Eaton, and R. Engel-Herbert, Adv. Mater. **25**, 3578 (2013).
[13]Y. Lan, X. Chen, and M. He, J. Alloys Compd. **354**, 95 (2003).
[14]G. Koster, L. Klein, W. Siemons, G. Rijnders, J. S. Dodge, C.-B. Eom, D. H. A. Blank, and M. R. Beasley, Rev. Mod. Phys. **84**, 253 (2012).
[15]Y. Kozuka, Y. Hikita, C. Bell, and H. Y. Hwang, Appl. Phys. Lett. **97**, 012107 (2010).
[16]A. Vailionis, W. Siemons, and G. Koster, Appl. Phys. Lett. **93**, 051909 (2008).
[17]M. Hiratani, C. Okazaki, K. Imagawa, and K. Takagi, Jpn. J. Appl. Phys., Part 1 **35**, 6212 (1996).
[18]G. Herranz, V. Laukhin, F. Sánchez, P. Levy, C. Ferrater, M. V. García-Cuenca, M. Varela, and J. Fontcuberta, Phys. Rev. B **77**, 165114 (2008).
[19]L. Zhang, Y. Zhou, L. Guo, W. Zhao, A. Barnes, H. Zhang, C. Eaton, Y. Zheng, M. Brahlek, H. F. Haneef, N. J. Podraza, M. H. W. Chan, V. Gopalan, K. M. Rabe, and R. Engel-Herbert, Nat. Mater. **15**, 204 (2016).
[20]K. Yoshimatsu, K. Okabe, H. Kumigashira, S. Okamoto, S. Aizaki, A. Fujimori, and M. Oshima, Phys. Rev. Lett. **104**, 147601 (2010).
[21]K. Yoshimatsu, K. Horiba, H. Kumigashira, T. Yoshida, A. Fujimori, and M. Oshima, Science **333**, 319 (2011).
[22]G. Koster, B. L. Kropman, G. J. H. M. Rijnders, D. H. A. Blank, and H. Rogalla, Appl. Phys. Lett. **73**, 2920 (1998).
[23]See https://physics.nist.gov/ for Nist atomic spectra database lines form.
[24]S. Stepanov, E. Kondrashkina, R. Köhler, D. Novikov, G. Materlik, and S. Durbin, Phys. Rev. B **57**, 4829 (1998).